Supplementary material

This appendix contains supplementary material that will posted on the public CDS record but would not be added in the paper. Figures are presented to facilitate the discussion of these results at conferences.

The comparison with the result from the ALICE collaboration in Fig. 3 shows that the two results are compatible. The result of this paper is also compared with the 2015 LHCb result in Fig. 2. The significance between these two measurements is calculated to be

$$\frac{|\sigma_{15} - \sigma_{18}|}{\sqrt{\sigma^2_{\sigma_{15}} + \sigma^2_{\sigma_{18}}}} = 2.038$$

using the value and uncertainty in the total rapidity interval $2.0 < y^* < 4.5$, where

$$\sigma_{18} = 5.965 \pm 0.059\,(\text{stat}) \pm 0.232\,(\text{syst}) \pm 0.262\,(\text{lumi})\,\text{mb}$$

from the 2018 result and

$$\sigma_{15} = 4.45 \pm 0.24\,(\text{stat}) \pm 0.18\,(\text{syst}) \pm 0.58\,(\text{lumi})\,\text{mb}$$

from the 2015 result [1]. The statistical, systematic and luminosity uncertainties were added in quadrature. The dominant uncertainty for the difference of these two result arises from the luminosity determination, The two results deviate by 2.038 standard deviations, corresponding to a p value of 0.021. The 13% luminosity uncertainty in the 2015 result is significantly larger than the 2018 result.

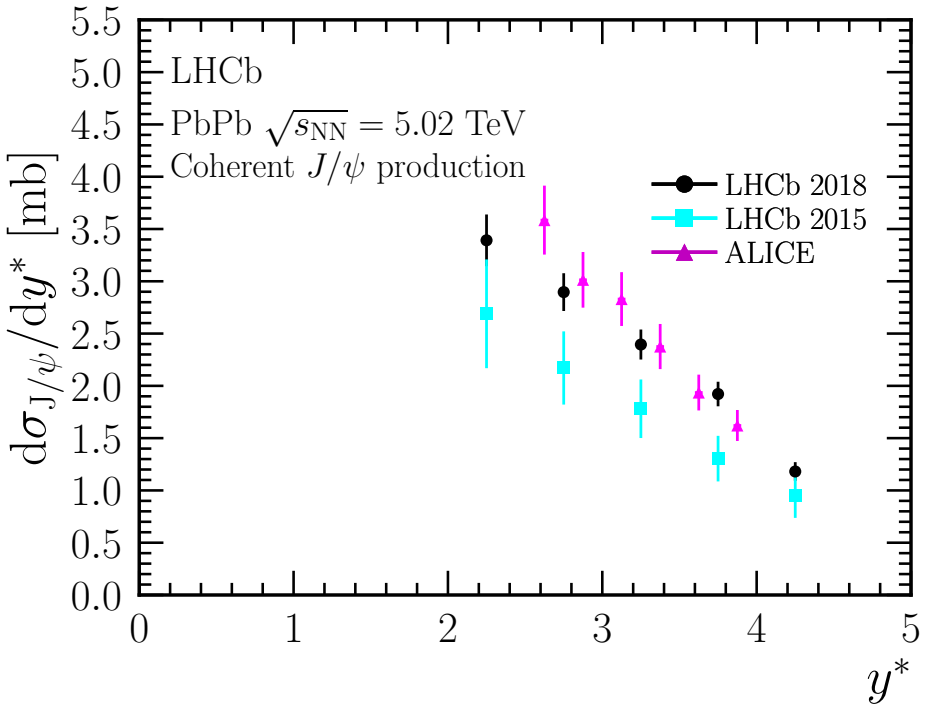

Figure 1: Differential cross-sections as a function of rapidity for coherent J/ψ production compared to the previous measurements at ALICE [2] and LHCb [1]. The measurements are shown as dots, squares and triangles, where the uncertainties represent total uncertainties respectively.

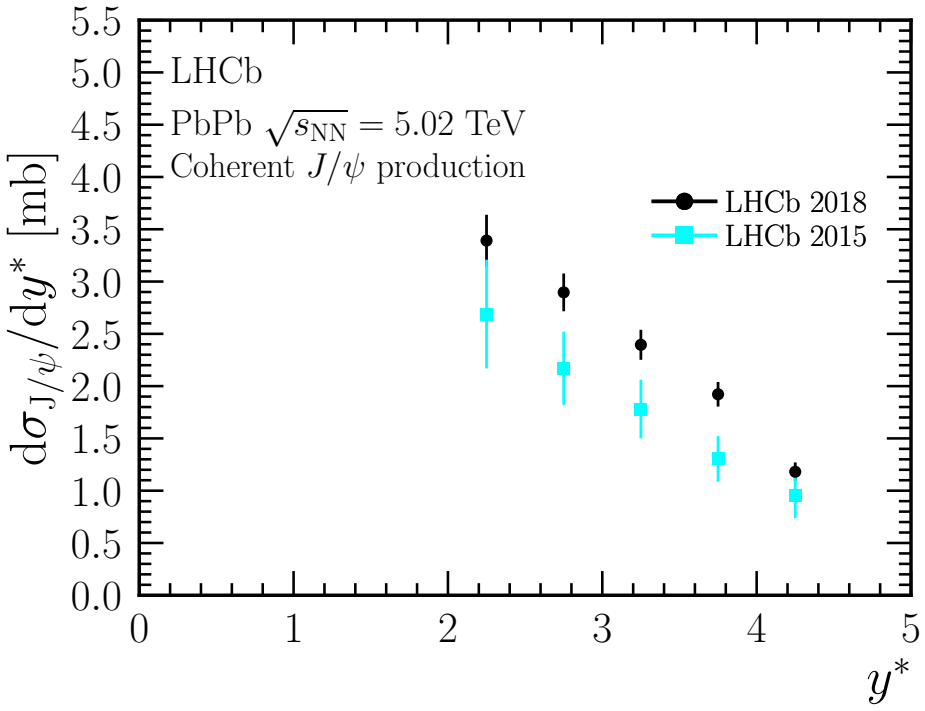

Figure 2: Differential cross-sections as a function of rapidity for coherent J/ψ production compared to the previous measurement at LHCb [1]. The measurements are shown as dots and squares, where the uncertainties represent total uncertainties respectively.

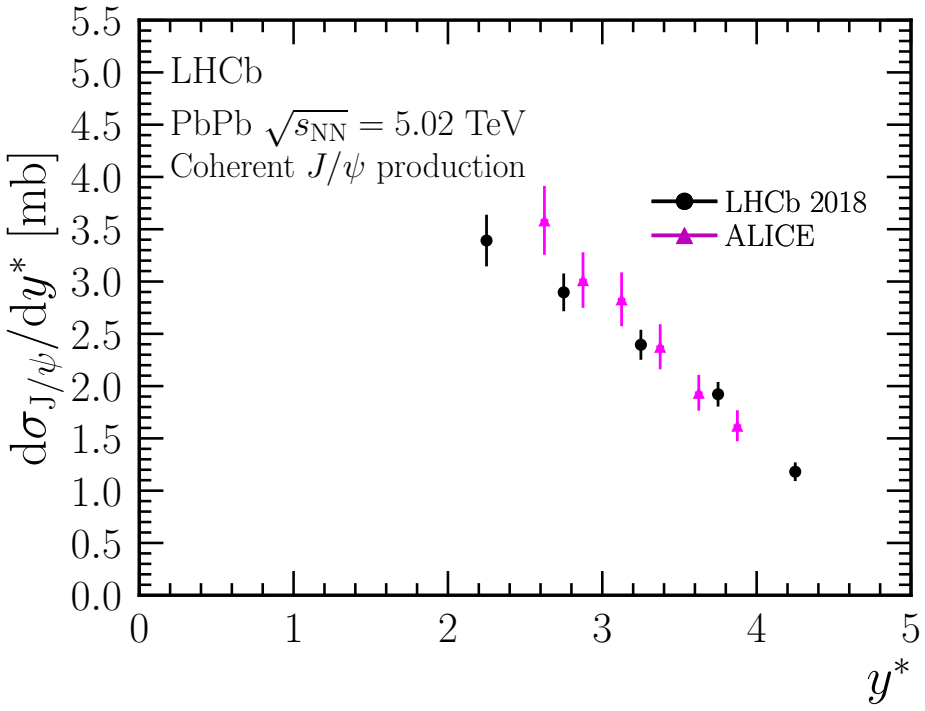

Figure 3: Differential cross-sections as a function of rapidity for coherent J/ψ production compared to the previous measurement at ALICE [2]. The measurements are shown as dots and triangles, where the uncertainties represent total uncertainties respectively.

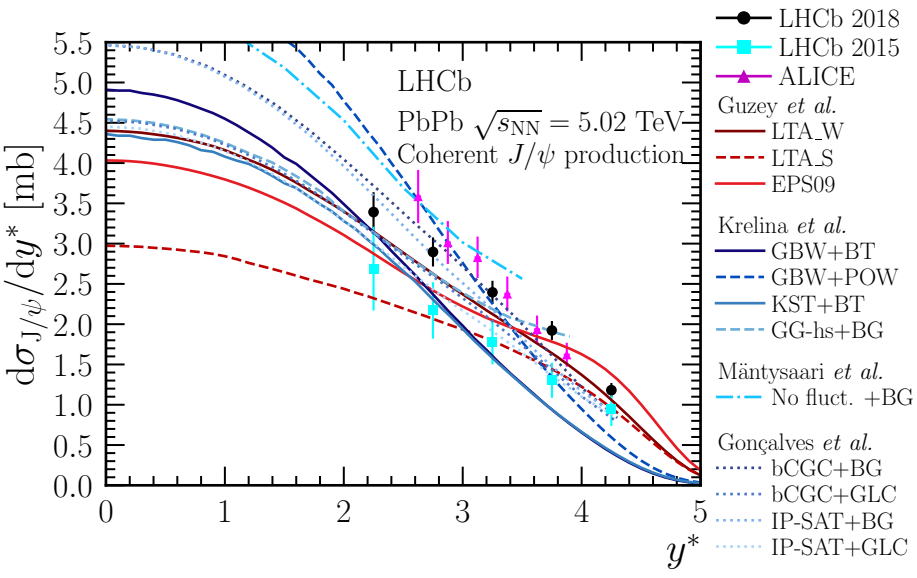

Figure 4: Differential cross-sections as a function of rapidity for coherent J/ψ production compared to the previous measurements at ALICE [2] and LHCb [1]. The measurements are shown as dots, squares and triangles, where the uncertainties represent total uncertainties respectively. Then all these results are compared to theoretical predictions [3–12].

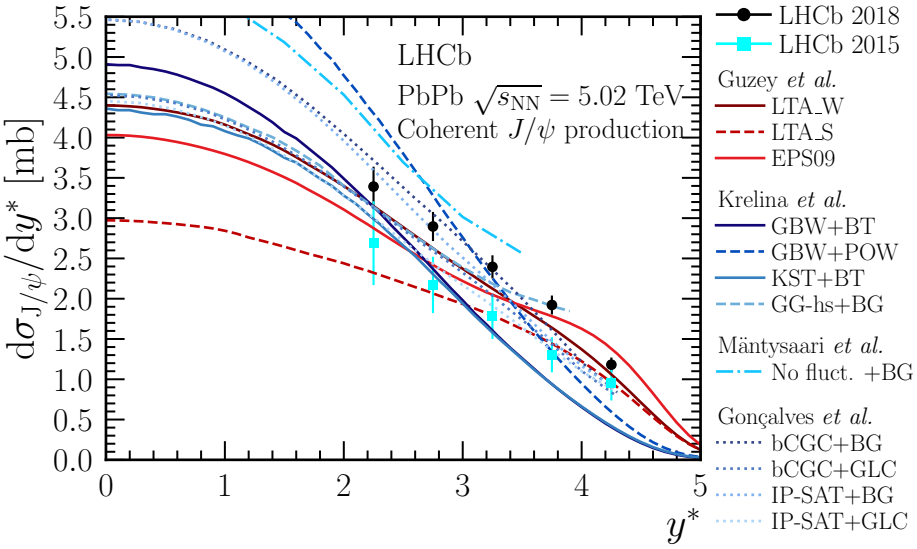

Figure 5: Differential cross-sections as a function of rapidity for coherent J/ψ production compared to the previous measurement at LHCb [1]. The measurements are shown as dots and squares, where the uncertainties represent total uncertainties respectively. Then both results are compared to theoretical predictions [3–12].

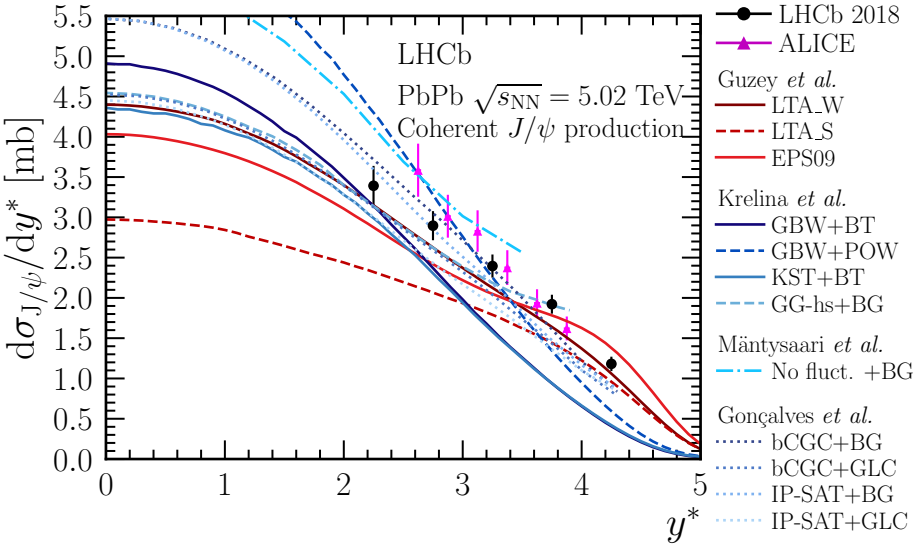

Figure 6: Differential cross-sections as a function of rapidity for coherent J/ψ production compared to the previous measurement at ALICE [2]. The measurements are shown as dots and triangles, where the uncertainties represent total uncertainties respectively. Then both results are compared to theoretical predictions [3–12].

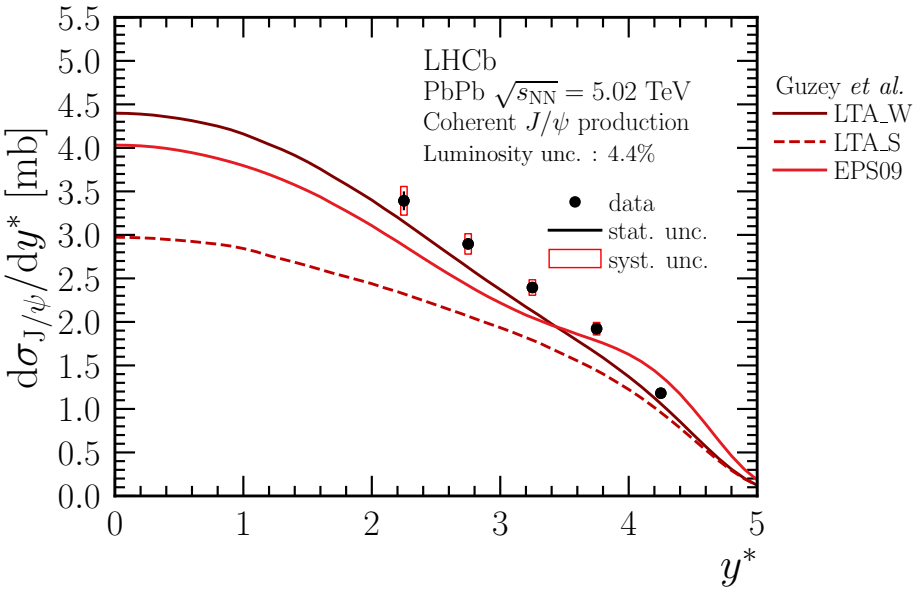

Figure 7: Differential cross-sections as a function of rapidity for coherent J/ψ production compared to NRQCD predictions [9].

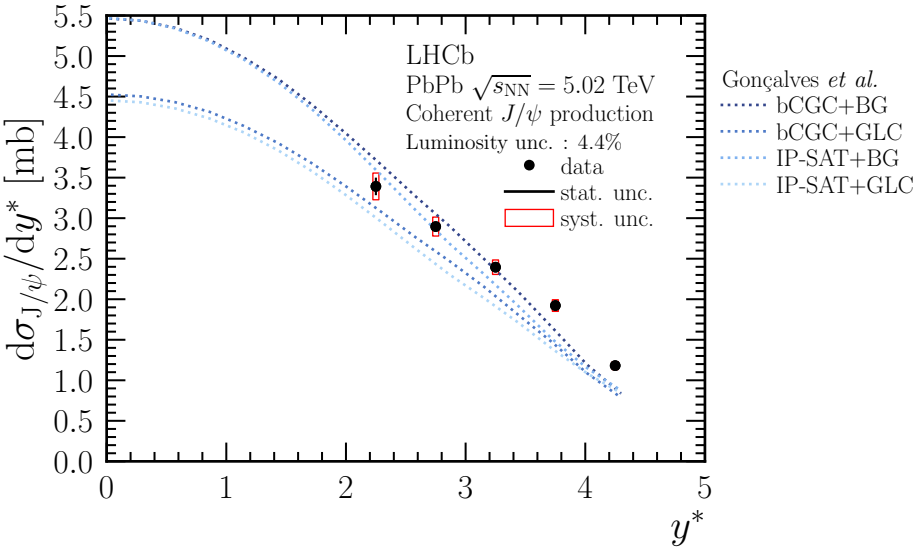

Figure 8: Differential cross-sections as a function of rapidity for coherent J/ψ production compared to Colour-Dipole based predictions using the boosted Gaussian (BG) wave function and the Gauss-LC (GLC) wave function [6, 7].

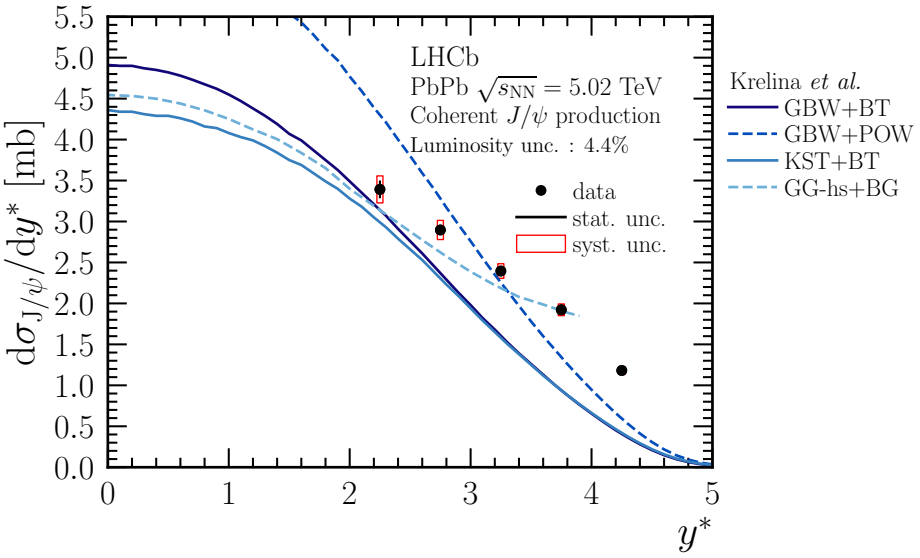

Figure 9: Differential cross-sections as a function of rapidity for coherent J/ψ production compared to Colour-Dipole based predictions from Ref. [4, 5].

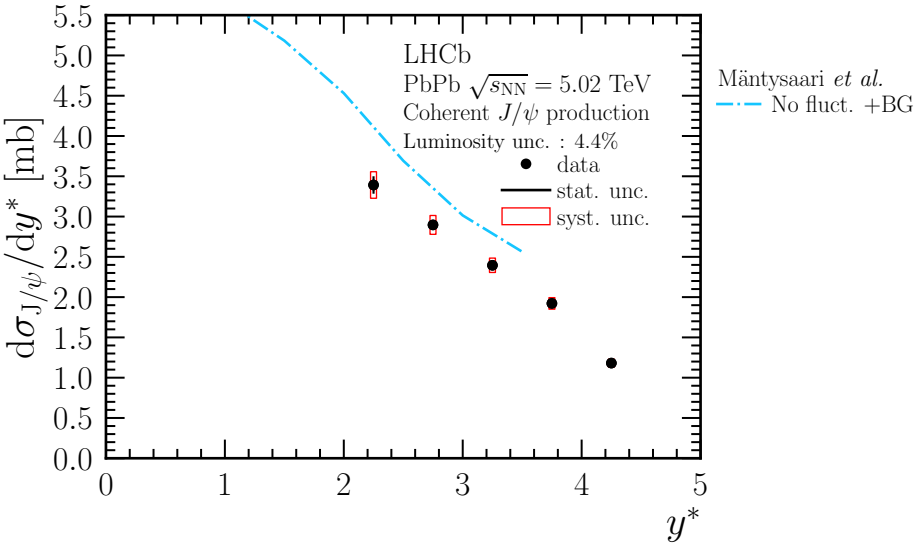

Figure 10: Differential cross-sections as a function of rapidity for coherent J/ψ production compared to Colour-Dipole based predictions with and without taking into account initial state fluctuations [8, 12].

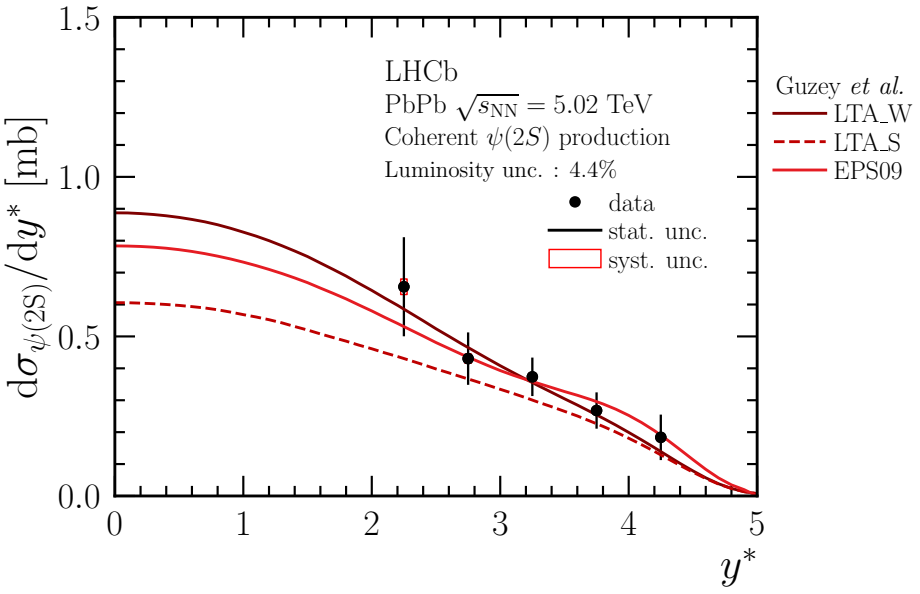

Figure 11: Differential cross-sections as a function of rapidity for coherent $\psi(2S)$ production compared to NRQCD predictions [9].

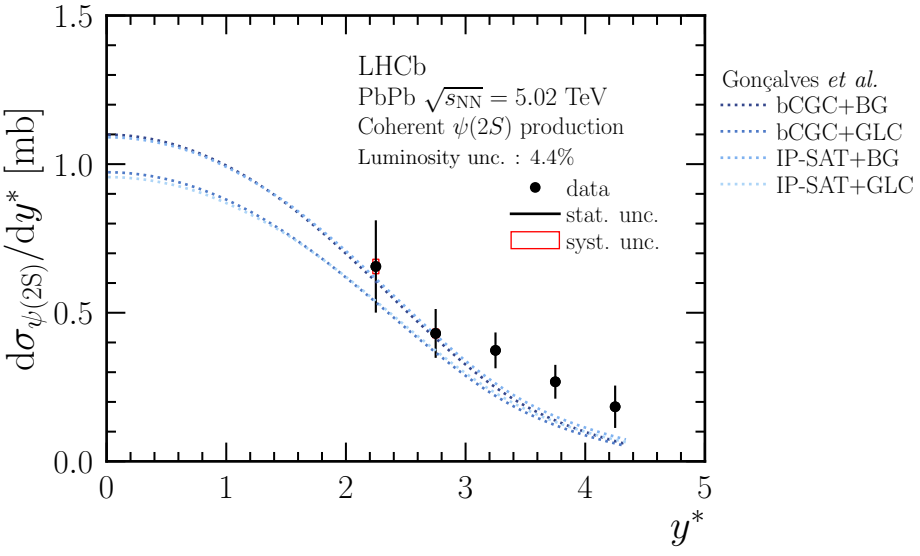

Figure 12: Differential cross-sections as a function of rapidity for coherent $\psi(2S)$ production compared to Colour-Dipole based predictions using the boosted Gaussian (BG) wave function and the Gauss-LC (GLC) wave function [6, 7].

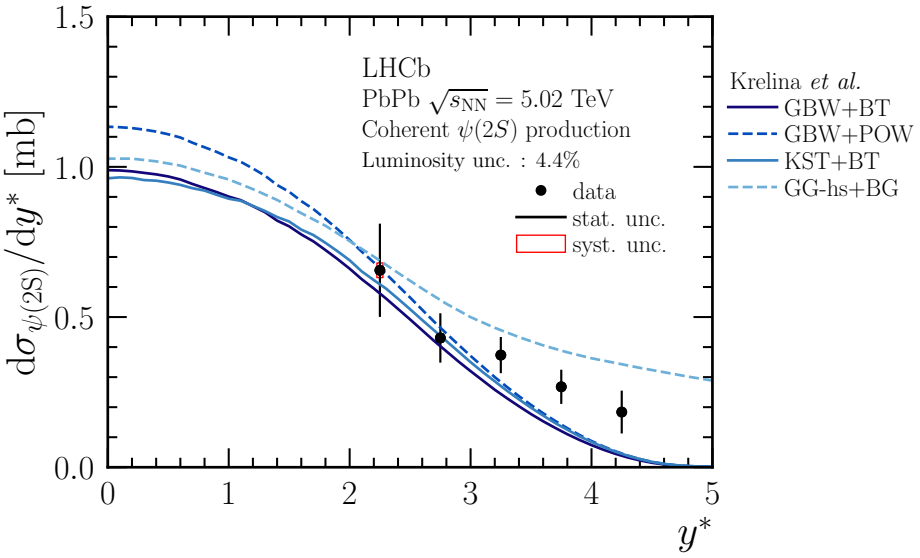

Figure 13: Differential cross-sections as a function of rapidity for coherent $\psi(2S)$ production compared to Colour-Dipole based predictions from Ref. [4, 5].

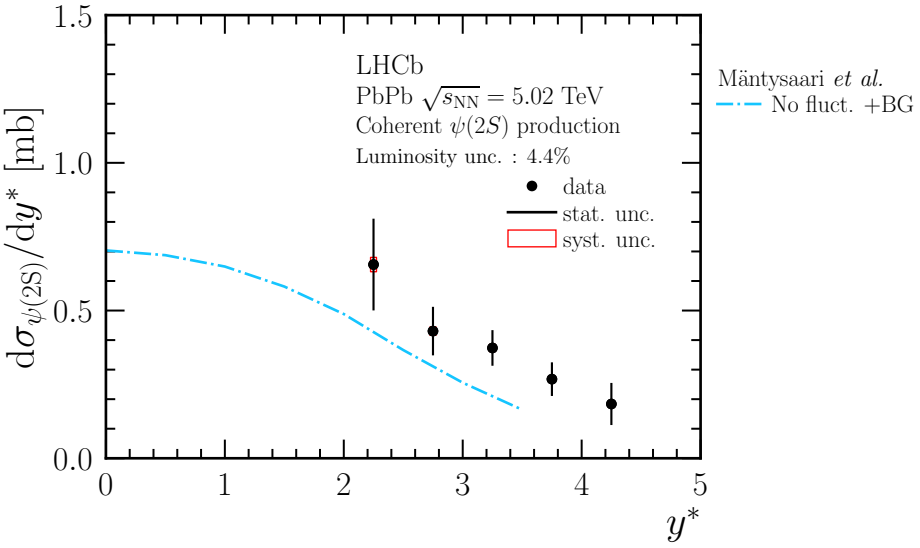

Figure 14: Differential cross-sections as a function of rapidity for coherent $\psi(2S)$ production compared to Colour-Dipole based predictions with and without taking into account initial state fluctuations [8, 12].

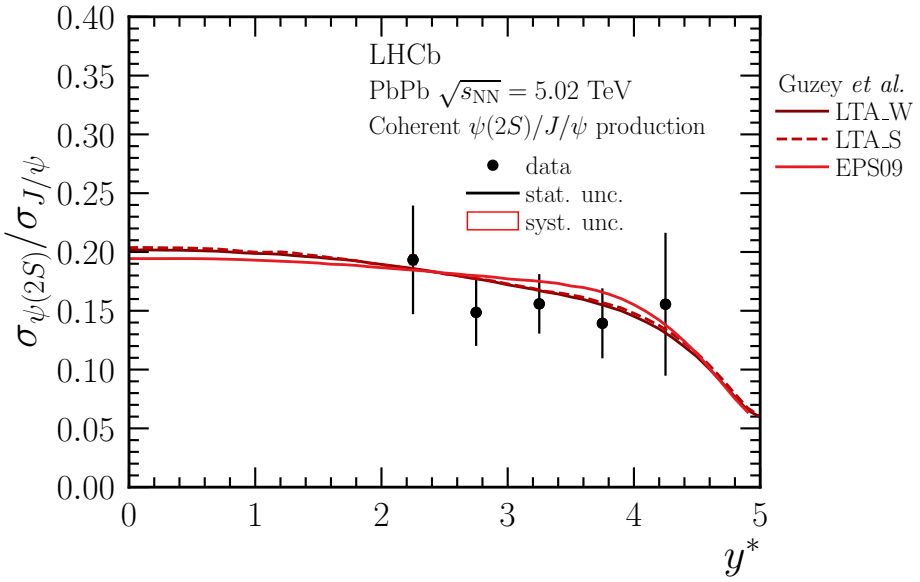

Figure 15: The ratio of differential cross-sections as a function of rapidity for coherent $\psi(2S)/J/\psi$ production compared to NRQCD predictions [9].

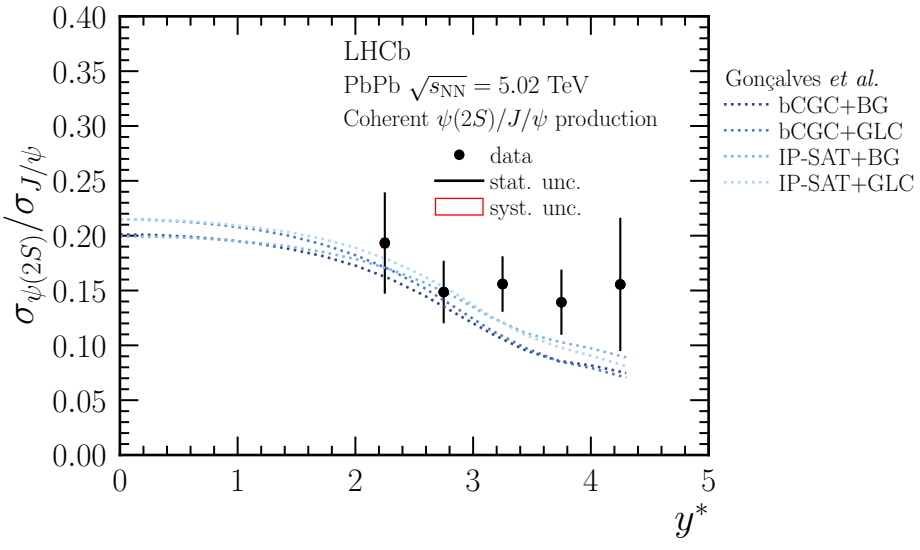

Figure 16: The ratio of differential cross-sections as a function of rapidity for coherent $\psi(2S)/J/\psi$ production compared to Colour-Dipole based predictions using the boosted Gaussian (BG) wave function and the Gauss-LC (GLC) wave function [6, 7].

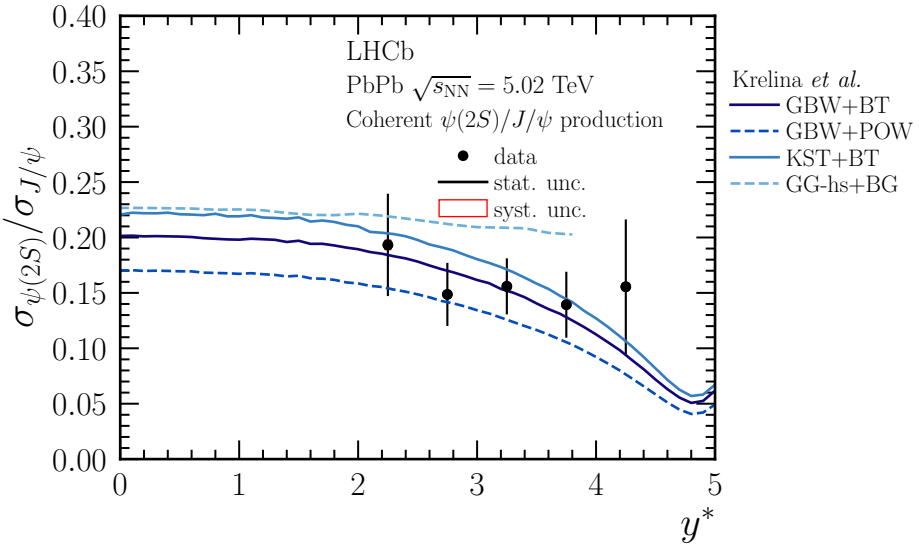

Figure 17: The ratio of differential cross-sections as a function of rapidity for coherent $\psi(2S)/J/\psi$ production compared to Colour-Dipole based predictions from Ref. [4, 5].

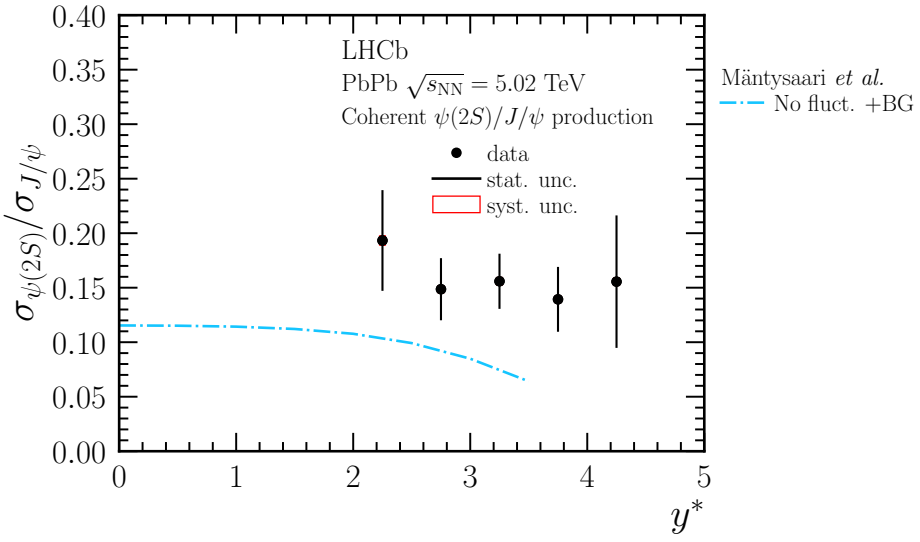

Figure 18: The ratio of differential cross-sections as a function of rapidity for coherent $\psi(2S)/J/\psi$ production compared to Colour-Dipole based predictions with and without taking into account initial state fluctuations [8, 12].

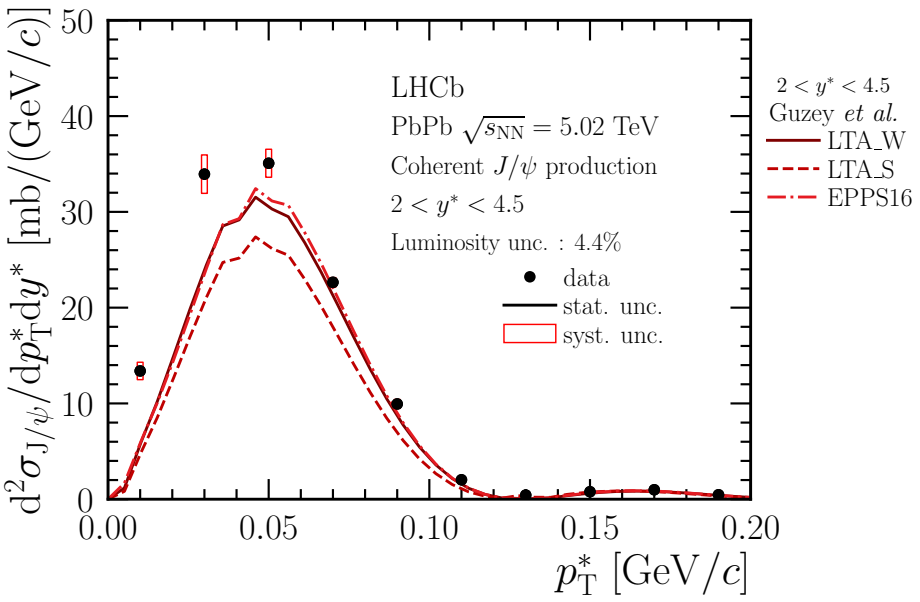

Figure 19: Double differential cross-sections as a function of p_{T}^* for coherent J/ψ production compared to NRQCD predictions [10].

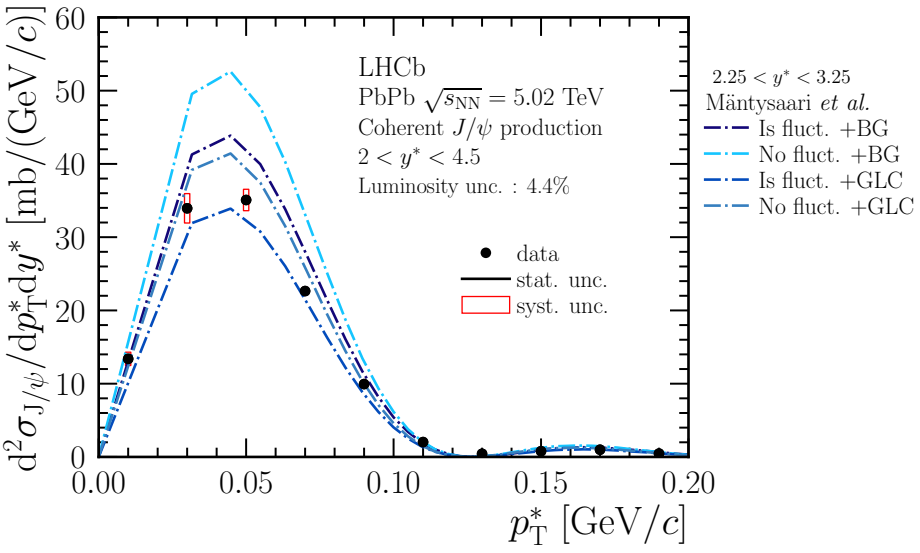

Figure 20: Double differential cross-sections as a function of p_{T}^* for coherent J/ψ production compared to Colour-Dipole based predictions with and without taking into account initial state fluctuations [11].

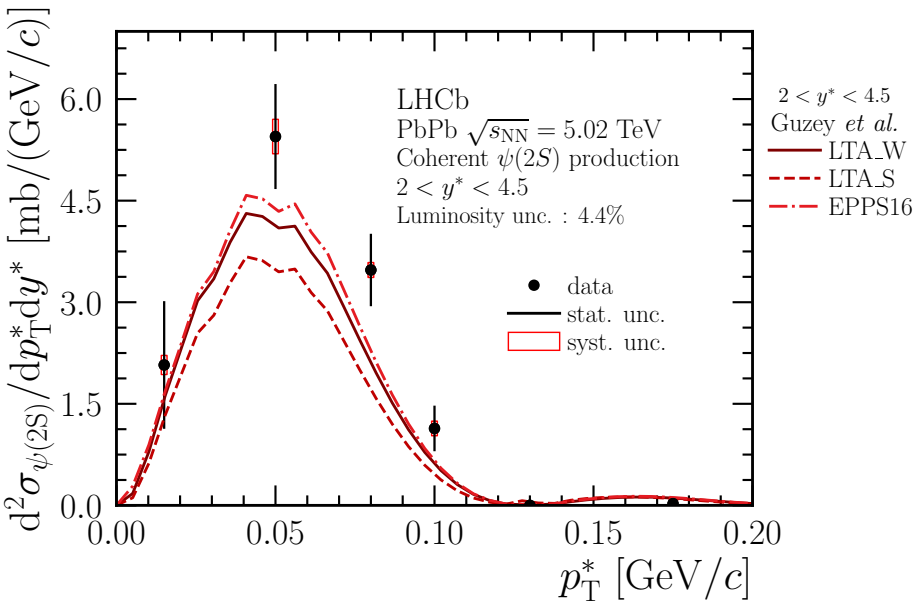

Figure 21: Double differential cross-sections as a function of $p_{\rm T}^*$ for coherent $\psi(2S)$ production compared to NRQCD predictions [10].

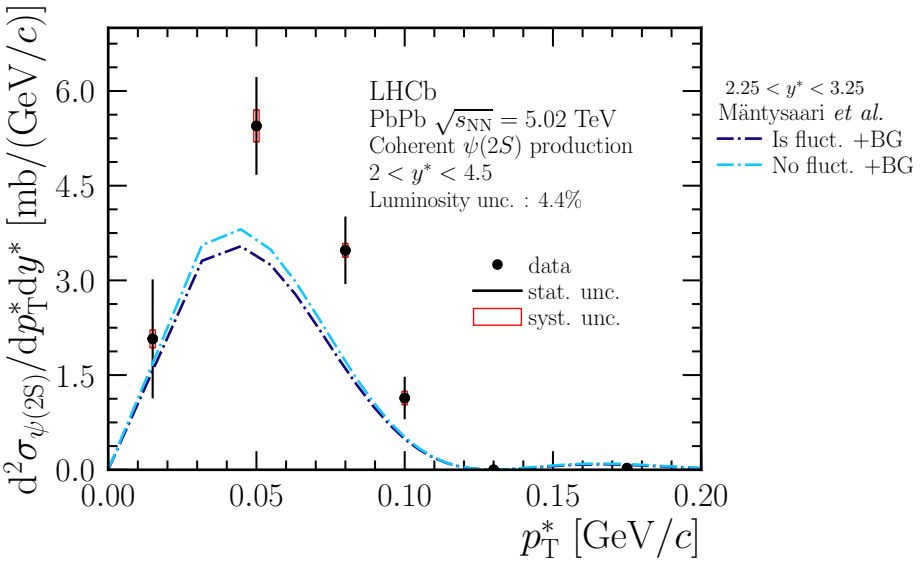

Figure 22: Double differential cross-sections as a function of $p_{\rm T}^*$ for coherent $\psi(2S)$ production compared to Colour-Dipole based predictions with and without taking into account initial state fluctuations [11].

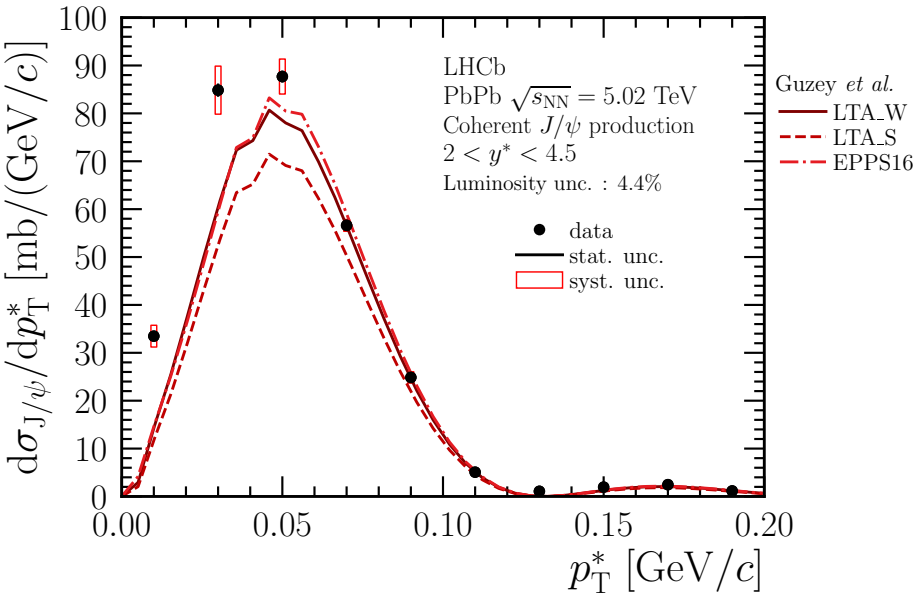

Figure 23: Differential cross-sections as a function of p_{T}^* for coherent J/ψ production compared to NRQCD predictions [10] in the rapidity range $2.0 < y^* < 4.5$.

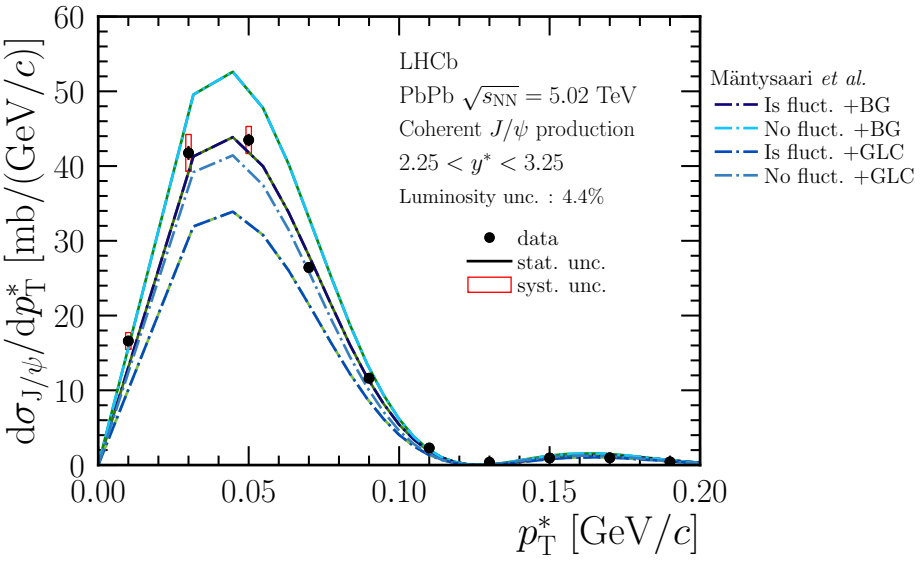

Figure 24: Differential cross-sections as a function of p_{T}^* for coherent J/ψ production compared to Colour-Dipole based predictions with and without taking into account initial state fluctuations [11] in the rapidity range $2.25 < y^* < 3.25$.

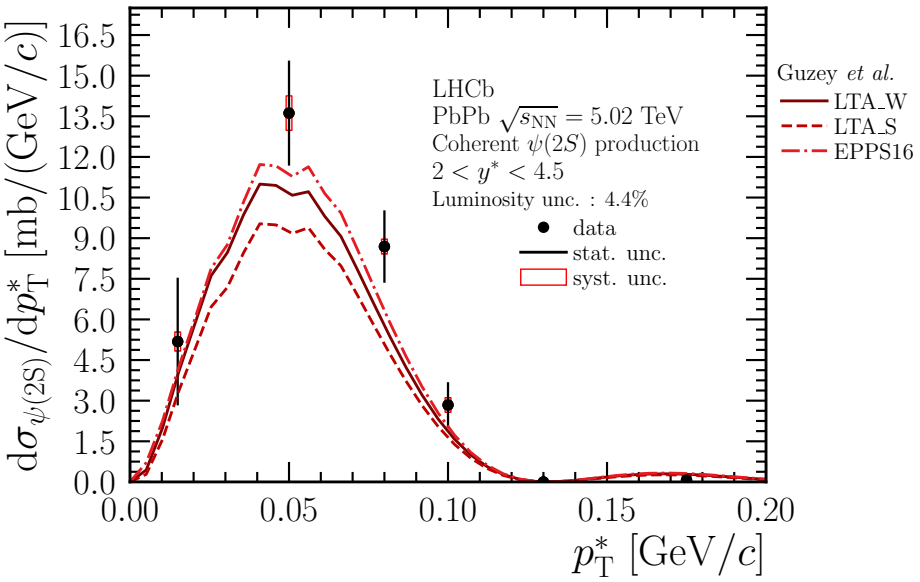

Figure 25: Differential cross-sections as a function of $p_{\rm T}^*$ for coherent $\psi(2S)$ production compared to NRQCD predictions [10] in the rapidity range $2.0 < y^* < 4.5$.

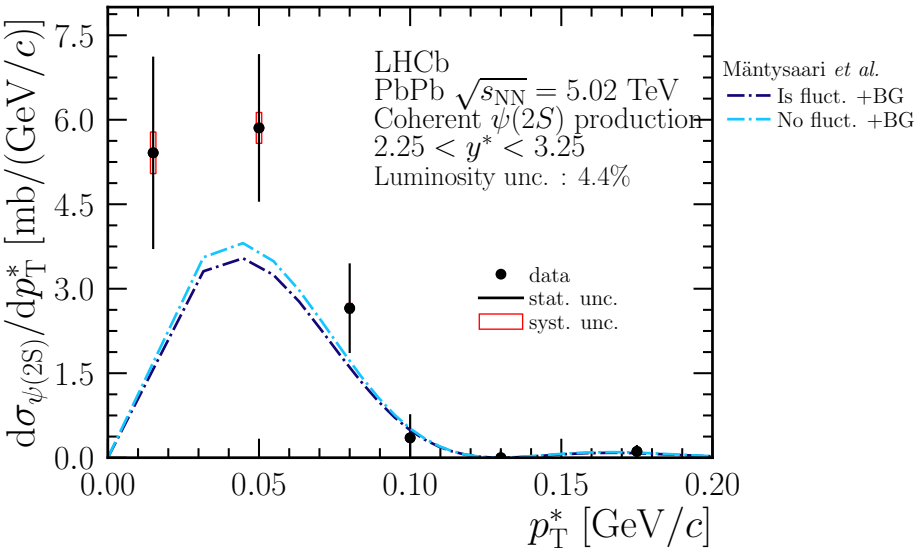

Figure 26: Differential cross-sections as a function of $p_{\rm T}^*$ for coherent $\psi(2S)$ production compared to Colour-Dipole based predictions with and without taking into account initial state fluctuations [11] in the rapidity range $2.25 < y^* < 3.25$.

Table 1: The differential cross-sections of coherent J/ψ production as a function of p_{T}^{*} in the rapidity range $2.0 < y^{*} < 4.5$.

Interval [MeV/c]	$\mathrm{d}\sigma_{J/\psi}^{\mathrm{coh}}/\mathrm{d}p_{\mathrm{T}}^{*}$ [mb/(GeV/c)]	Uncertainties [mb/(GeV/c)]			
		Stat.	Syst.	Lumi.	Total
$0 < p_{\mathrm{T}}^{*} < 20$	33.478	0.881	2.271	1.468	2.844
$20 < p_{\mathrm{T}}^{*} < 40$	84.851	1.389	5.017	3.721	6.399
$40 < p_{\mathrm{T}}^{*} < 60$	87.692	1.237	3.655	3.846	5.448
$60 < p_{\mathrm{T}}^{*} < 80$	56.613	0.952	1.229	2.483	2.930
$80 < p_{\mathrm{T}}^{*} < 100$	24.862	0.622	1.180	1.090	1.722
$100 < p_{\mathrm{T}}^{*} < 120$	5.071	0.319	0.777	0.222	0.869
$120 < p_{\mathrm{T}}^{*} < 140$	1.081	0.209	0.346	0.047	0.407
$140 < p_{\mathrm{T}}^{*} < 160$	1.953	0.256	0.682	0.086	0.734
$160 < p_{\mathrm{T}}^{*} < 180$	2.465	0.295	0.532	0.108	0.618
$180 < p_{\mathrm{T}}^{*} < 200$	1.159	0.256	0.199	0.051	0.328
$0 < p_{\mathrm{T}}^{*} < 200$	29.759	0.258	0.583	1.305	1.452

Table 2: The differential cross-sections of coherent J/ψ production as a function of p_{T}^{*} in the rapidity range $2.25 < y^{*} < 3.25$.

Interval [MeV/c]	$\mathrm{d}\sigma_{J/\psi}^{\mathrm{coh}}/\mathrm{d}p_{\mathrm{T}}^{*}$ [mb/(GeV/c)]	Uncertainties [mb/(GeV/c)]			
		Stat.	Syst.	Lumi.	Total
$0 < p_{\mathrm{T}}^{*} < 20$	16.597	0.598	1.127	0.728	1.469
$20 < p_{\mathrm{T}}^{*} < 40$	41.758	0.932	2.471	1.831	3.214
$40 < p_{\mathrm{T}}^{*} < 60$	43.486	0.831	1.815	1.907	2.761
$60 < p_{\mathrm{T}}^{*} < 80$	26.437	0.614	0.578	1.159	1.434
$80 < p_{\mathrm{T}}^{*} < 100$	11.619	0.403	0.553	0.509	0.853
$100 < p_{\mathrm{T}}^{*} < 120$	2.281	0.201	0.350	0.100	0.415
$120 < p_{\mathrm{T}}^{*} < 140$	0.371	0.127	0.119	0.016	0.175
$140 < p_{\mathrm{T}}^{*} < 160$	0.947	0.166	0.331	0.041	0.372
$160 < p_{\mathrm{T}}^{*} < 180$	0.969	0.181	0.209	0.042	0.280
$180 < p_{\mathrm{T}}^{*} < 200$	0.423	0.172	0.073	0.018	0.188
$0 < p_{\mathrm{T}}^{*} < 200$	14.369	0.171	0.282	0.630	0.711

Table 3: The differential cross-sections of coherent $\psi(2S)$ production as a function of p_{T}^{*} in the rapidity range $2.0 < y^{*} < 4.5$.

Interval [MeV/c]	$\mathrm{d}\sigma^{\mathrm{coh}}_{\psi(2S)}/\mathrm{d}p_{\mathrm{T}}^{*}$ [mb/(GeV/c)]	Uncertainties [mb/(GeV/c)]			
		Stat.	Syst.	Lumi.	Total
$0 < p_{\mathrm{T}}^{*} < 30$	5.183	2.356	0.352	0.227	2.393
$30 < p_{\mathrm{T}}^{*} < 70$	13.617	1.938	0.636	0.597	2.126
$70 < p_{\mathrm{T}}^{*} < 90$	8.690	1.337	0.275	0.381	1.417
$90 < p_{\mathrm{T}}^{*} < 110$	2.840	0.841	0.270	0.124	0.892
$110 < p_{\mathrm{T}}^{*} < 150$	0.000	0.233	0.000	0.000	0.233
$150 < p_{\mathrm{T}}^{*} < 200$	0.064	0.128	0.014	0.003	0.129
$0 < p_{\mathrm{T}}^{*} < 200$	4.583	0.401	0.131	0.201	0.468

Table 4: The differential cross-sections of coherent $\psi(2S)$ production as a function of p_{T}^{*} in the rapidity range $2.25 < y^{*} < 3.25$.

Interval [MeV/c]	$\mathrm{d}\sigma^{\mathrm{coh}}_{\psi(2S)}/\mathrm{d}p_{\mathrm{T}}^{*}$ [mb/(GeV/c)]	Uncertainties [mb/(GeV/c)]			
		Stat.	Syst.	Lumi.	Total
$0 < p_{\mathrm{T}}^{*} < 30$	5.413	1.708	0.368	0.237	1.764
$30 < p_{\mathrm{T}}^{*} < 70$	5.855	1.310	0.274	0.257	1.363
$70 < p_{\mathrm{T}}^{*} < 90$	2.654	0.796	0.084	0.116	0.809
$90 < p_{\mathrm{T}}^{*} < 110$	0.353	0.420	0.034	0.015	0.421
$110 < p_{\mathrm{T}}^{*} < 150$	0.000	0.126	0.000	0.000	0.126
$150 < p_{\mathrm{T}}^{*} < 200$	0.111	0.115	0.025	0.005	0.118
$0 < p_{\mathrm{T}}^{*} < 200$	2.220	0.269	0.172	0.097	0.334

References

[1] LHCb collaboration, R. Aaij *et al.*, *Study of coherent J/ψ production in lead-lead collisions at $\sqrt{s_{NN}} = 5TeV$*, arXiv:2107.03223.

[2] ALICE collaboration, S. Acharya *et al.*, *Coherent J/ψ photoproduction at forward rapidity in ultra-peripheral Pb-Pb collisions at $\sqrt{s_{\rm NN}} = 5.02$ TeV*, Phys. Lett. **B798** (2019) 134926, arXiv:1904.06272.

[3] V. P. Gonçalves and M. V. T. Machado, *Vector meson production in coherent hadronic interactions: an update on predictions for RHIC and LHC*, Phys. Rev. **C84** (2011) 011902, arXiv:1106.3036.

[4] J. Cepila, J. G. Contreras, and M. Krelina, *Coherent and incoherent* J/ψ *photonuclear production in an energy-dependent hot-spot model*, Phys. Rev. **C97** (2018) 024901, arXiv:1711.01855.

[5] B. Z. Kopeliovich, M. Krelina, J. Nemchik, and I. K. Potashnikova, *Heavy quarkonium production in ultraperipheral nuclear collisions*, arXiv:2008.05116.

[6] V. P. Gonçalves *et al.*, *Color dipole predictions for the exclusive vector meson photoproduction in pp,* pPb*, and* PbPb *collisions at run2 LHC energies*, Phys. Rev. **D96** (2017) 094027, arXiv:1710.10070.

[7] V. P. Gonçalves and M. V. T. Machado, *The QCD pomeron in ultraperipheral heavy ion collisions: IV. Photonuclear production of vector mesons*, Eur. Phys. J. **C40** (2005) 519, arXiv:hep-ph/0501099.

[8] H. Kowalski, L. Motyka, and G. Watt, *Exclusive diffractive processes at HERA within the dipole picture*, Phys. Rev. **D74** (2006) 074016, arXiv:hep-ph/0606272.

[9] V. Guzey, E. Kryshen, and M. Zhalov, *Coherent photoproduction of vector mesons in ultraperipheral heavy ion collisions: Update for run2 at the CERN Large Hadron Collider*, Phys. Rev. **C93** (2016) 055206, arXiv:1602.01456.

[10] V. Guzey, M. Strikman, and M. Zhalov, *Accessing transverse nucleon and gluon distributions in heavy nuclei using coherent vector meson photoproduction at high energies in ion ultraperipheral collisions*, Phys. Rev. **C95** (2017) 025204, arXiv:1611.05471.

[11] T. Lappi and H. Mäntysaari, *Diffractive vector meson production in ultraperipheral heavy ion collisions from the color glass condensate*, PoS **DIS2014** (2014) 069, arXiv:1406.2877.

[12] H. Mäntysaari and B. Schenke, *Probing subnucleon scale fluctuations in ultraperipheral heavy ion collisions*, Phys. Lett. **B772** (2017) 832, arXiv:1703.09256.